

# An Actuated Universal Joint using the Twisted String Actuator: Design and Experimentation

Damian Crosby, Joaquin Carrasco, *Member, IEEE*, William Heath, *Member, IEEE*, and Andrew Weightman

**Abstract**—Actuated universal joints, or equivalent joint systems, are found in a number of robotic applications, in particular mobile snake robots, snake-arm robots and robotic tails. Such joints use a variety of actuation methods, including direct drive motors, linear screw drives, cable based systems, and hydraulics/pneumatics. In this paper the authors design and create a mechanism that uses the Twisted String Actuator (TSA) in an antagonistic triad to actuate the universal joint, using orientation sensors to create a robust closed loop control system. Various experiments then defined the performance of the system. This results in a compact high performance actuation system that exploits the properties of TSA to give it various advantages over existing actuation methods.

*Index Terms*—???

## I. INTRODUCTION

Actuated Universal Joint (AUJ) mechanisms are found in a wide range of robotic applications, such as confined space inspection using snake-arm robots [1], highly manoeuvrable mobile snake robots [2], and biomimetic robot tails for stability [3]. Mobile snake robots must usually incorporate electric actuators inline with their joints. This results in an AUJ having to shift the mass of the follower segments and all the actuators inside the follower segments, which results in high torque requirements and therefore Snake-arm robots and robotic tails can reduce the mass and size of the AUJ by moving their actuators away from the AUJs and use cables to transfer the force to the joints, or use hydraulic or pneumatic actuators which tend to be lighter than equivalent electric motors, at the expense of increased mass and bulk at the base of the arm or tail.

First developed by [4] in 2010, the Twisted String Actuator (TSA) uses two or more strings between two fixtures as a linear actuator. When one fixture is rotated (typically by an electric motor), the looped string twists into a helix, decreasing the distance between them. Equation 2 calculates the distance  $l_s$  for a two string system with infinite stiffness for a given rotation angle  $\theta_s$ , where  $l_u$  is the unwound length between the fixtures and  $r_s$  is half the string thickness.

The primary advantage of TSA over similar linear actuators such as a leadscrew is the reduction the TSA provides is not proportional (or even slightly inversely proportional) to the mass of the actuator. By decreasing  $r_s$  (or  $r_s + r_c$  when there are more than two strings, where  $r_c$  is the “core radius”, or half the gap between any two strings that intersects the axis of rotation) the reduction increases for a constant  $l_u$  and  $\theta_s$ , resulting in a greater reduction with no increase, or even a slight decrease, in actuator mass. While the reduction in a

leadscrew can be increased by decreasing the lead on the thread (typically denoted as  $\lambda$ ) which also has no increase in mass, this has a limited range and can quickly run up against manufacturing tolerances or material strength requirements. In order to achieve greater or more robust reductions, the screw radius has to be increased, or the driving motor has to have a larger reduction before driving the screw, both of which usually result in more material (typically steel) and therefore more mass.

However, TSA does have some drawbacks, the most significant of which is a non-linear reduction equation, which is also dependent on the motor angle  $\theta_s$  (and therefore actuator position). The reduction decreases in a non-linear fashion as the angle increases, with the derivative decreasing as the angle increases. There is also the compliance of the strings to consider, depending on the thickness and material chosen, which becomes a significant factor under high forces. Both of these issues can be addressed with accurate modelling [5] and/or a robust control strategy, as demonstrated in [4]. What is perhaps more an issue regarding mass for an AUJ is the unidirectional force of the TSA, which can only impart force in tension. This means that for an AUJ, a minimum of three TSA are required unless spring return mechanisms are used, which would impart additional force on the TSA and therefore reduce performance. However, the potential high force to mass ratio of the TSA due to the non-proportional reduction may adequately compensate for the additional actuator requirement.

The focus of this research is to discover if the TSA is a suitable candidate for control of an AUJ considering both the benefits and drawbacks. To this end, the first objective is to simulate a model and then construct a physical experimental prototype to validate the proposed control system. Then, the second objective is to compare the results from both the simulation and experimental prototype with other inline actuation methods for an AUJ to analyse and discuss the potential advantages and disadvantages of TSA actuation against alternatives.

### A. Antagonistic Triad

As mentioned in the introduction, because the TSA provides only tensile force, a minimum of three actuators are required. These can be arranged in a triangular configuration to create an “antagonistic triad”, akin to the antagonistic pairs of muscles found in animals. Where a revolute joint would be found between the connecting ends of the actuator, a universal joint is found instead. The geometric structure of the system can

0000-0000/00\$00.00 © 2000 IEEE with two equilateral triangles of inradius  $r$  on

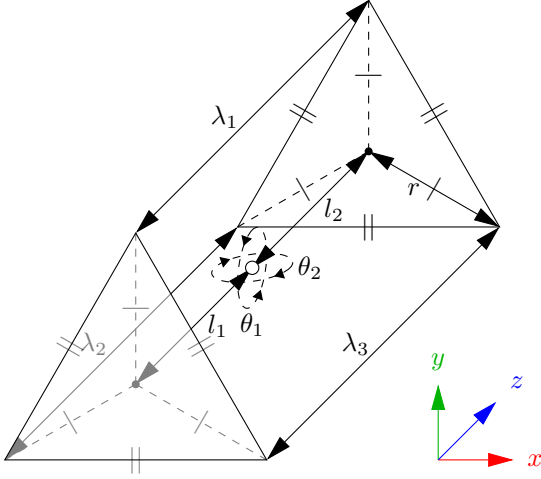


Fig. 1: Kinematic diagram of the antagonistic triad.

two planes separated in the  $z$  axis. The centroids are then connected via a universal joint from each plane normal to an intersecting point, described by vector  $\theta = [\theta_1 \ \theta_2]$  to denote the rotation of the second plane relative to the first, in the  $x$  and  $y$  axis around the intersecting point, and  $l_1$  and  $l_2$  to denote the normal distance from the intersection to the first and second plane centroids respectively. When  $\theta = [0 \ 0]$  the triangles are parallel to each other. The distance between the vertex pairs of each triangle is then denoted as  $[\lambda_1 \ \lambda_2 \ \lambda_3]$  for the “top”, “left” and “right” vertices of the triangles. When  $\theta$  is changed, this will change  $\lambda_1$ ,  $\lambda_2$  and  $\lambda_3$  respectively. A diagram of this is shown in figure 1.

To calculate the lengths of the strings for a given  $\theta$  of the universal joint, we can define a vector function  $\Lambda(\theta) = [\lambda_1(\theta) \ \lambda_2(\theta) \ \lambda_3(\theta)]$  with  $l_1$ ,  $l_2$  and  $r$  as the coefficients, where the scalar functions are defined in equation 1.

The geometric structure of the system can be described with two equilateral triangles of circumscribed radius  $r$  on two planes separated in the  $z$  axis. The centroids are then connected via a universal joint from each plane normal to an intersecting point, described by vector  $\theta = [\theta_1 \ \theta_2]$  to denote the rotation of the second plane relative to the first, in the  $x$  and  $y$  axis around the intersecting point, and  $l_1$  and  $l_2$  to denote the normal distance from the intersection to the first and second plane centroids respectively. When  $\theta = [0 \ 0]$  the triangles are parallel to each other. The distance between the vertex pairs of each triangle is then denoted as  $[\lambda_1 \ \lambda_2 \ \lambda_3]$  for the “top”, “left” and “right” vertices of the triangles. When  $\theta$  is changed, this will change  $\lambda_1$ ,  $\lambda_2$  and  $\lambda_3$  respectively. A diagram of this is shown in figure 1.

To calculate the lengths of the strings for a given  $\theta$  of the AUJ, we can define a vector function  $\Lambda(\theta) = [\lambda_1(\theta) \ \lambda_2(\theta) \ \lambda_3(\theta)]$  with  $l_1$ ,  $l_2$  and  $r$  as the coefficients, where the scalar functions are defined in equation 1.

$$\begin{aligned} \lambda_1(\theta) &= \sqrt{(l_1 + l_2 \cos \theta_1 \cos \theta_2 + r \cos \theta_1 \sin \theta_2)^2 \\ &\quad + (r - r \cos \theta_2 + l_2 \sin \theta_2)^2 \\ &\quad + (l_2 \cos \theta_2 \sin \theta_1 + r \sin \theta_1 \sin \theta_2)^2} \\ \lambda_2(\theta) &= \sqrt{(a - b + c)^2 + (l_1 - d)^2 + (e)^2} \\ \lambda_3(\theta) &= \sqrt{(a + b - c)^2 + (l_1 + d)^2 + (e)^2} \end{aligned} \quad (1)$$

where:

$$\begin{aligned} a &= -\frac{\sqrt{3}r(\cos \theta_1 - 1)}{2} \\ b &= l_2 \cos \theta_2 \sin \theta_1 \\ c &= \frac{r \sin \theta_1 \sin \theta_2}{2} \\ d &= \frac{\sqrt{3}r \sin \theta_1}{2} + l_2 \cos \theta_1 \cos \theta_2 - \frac{r \cos \theta_1 \sin \theta_2}{2} \\ e &= \frac{r \cos \theta_2}{2} - \frac{r}{2} + l_2 \sin \theta_2 \end{aligned}$$

These were simply calculated by computing the transformation matrix for each string from one end to the other in cartesian coordinates, then acquiring the Euclidean norm of the resulting translation vector  $\| [x_n \ y_n \ z_n] \|_2$ .

### B. Twisted String Actuator

First developed by [4] in 2010, TSA uses two or more strings between two fixtures as a linear actuator. When one fixture is rotated (typically by an electric motor), the strings twist into a helix, decreasing the distance between the fixtures.

Equation 2 from [4] calculates the actuator length  $l_s$  for a given  $\theta_s$ , given  $l_u$  and  $r_s$  for a two string TSA. This equation assumes an infinite string stiffness, so is only reasonably accurate under low tension.

$$l_s(\theta_s) = \sqrt{l_u^2 - \theta_s^2 r_s^2} \quad (2)$$

Although theoretically the stroke of the TSA can be the entire domain of  $[0, l_n]$ , in reality the thickness of the string prevents a geometric helix from forming once the helix pitch  $q < 4r_s$  (or  $q < 2nr_s$  for  $n$  strings). This limits the lower bound of the stroke to the value calculated by equation 3, or approximately 46% of  $l_n$  for a two string TSA.

$$l_{min} = \frac{l_u}{\sqrt{\frac{\pi^2}{2} + 1}} \approx 0.46 l_u \quad (3)$$

## II. CONTROL SYSTEM

The control system is a four layer cascade design, using feedback of the joint position from the accelerometers and TSA force from the load cells. It uses a second order setpoint trajectory  $q$  as input, which can either be pre-defined or generated dynamically from user input. Feedback is provided by the AUJ angular position  $\theta$ , angular velocity  $\dot{\theta}$ , and TSA tension force  $f$ .

- 1)  $C_1$  AUJ Position PID Controller
- 2)  $C_2$  Inverse Dynamics
- 3)  $C_3$  TSA Force Optimisation Algorithm
- 4)  $C_4$  TSA Force P Controller

Functions  $C_{1...4}$  are then combined into a cascade function  $C_4(C_3(C_2(C_1(\dots), \dots), \dots), \dots), \dots)$ .

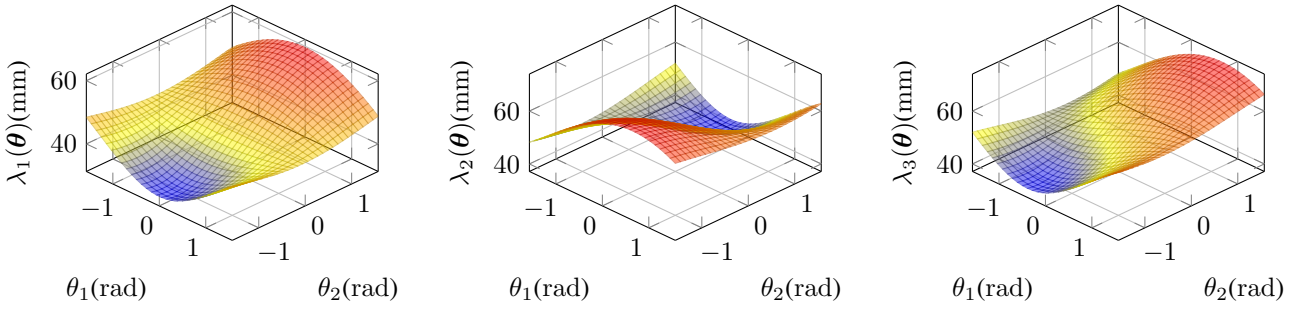


Fig. 2: Surface plots of each element of the vector function  $\Lambda(\theta)$ , assuming coefficient values from table I.

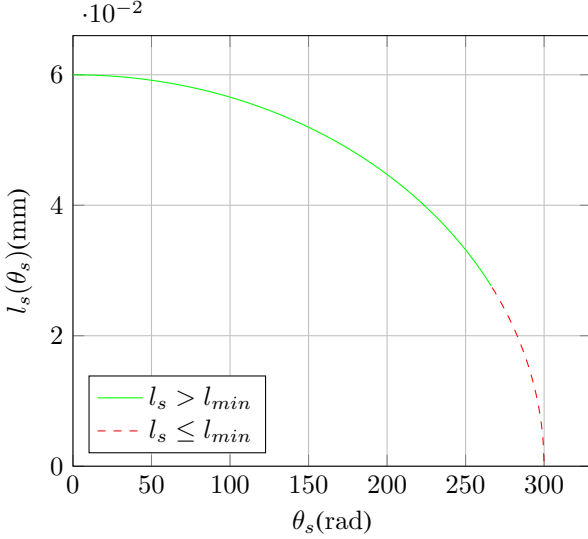


Fig. 3: TSA string length against motor angle with coefficients from table I.

#### A. AUJ Position PID Controller

This function is a PID controller with the input  $q$  as the setpoint and the AUJ angular position  $\theta$  and velocity  $\dot{\theta}$  as feedback, plus the addition of a feedforward term for the input acceleration  $\ddot{q}$ .

$$\begin{aligned}\epsilon &= q - \theta \\ \dot{\epsilon} &= \dot{q} - \dot{\theta}\end{aligned}\quad (4)$$

$$C_1(q, \dot{q}, \ddot{q}, \theta, \dot{\theta}) = K_P \epsilon + K_I \int_0^t \epsilon dt + K_D \dot{\epsilon} + \ddot{q}$$

In the discrete implementation used for fixed step simulation and experimental model control, the integral term is replaced by the trapezoidal rule.

$$K_I \int_0^t \epsilon \approx \sum_{i=0}^N \frac{\epsilon(t_i) + \epsilon(t_{i-1})}{2} \Delta t \quad (5)$$

#### B. Inverse Dynamics

This function converts the control signal from  $C_1$  to the desired AUJ torque using the Euler-Lagrange method in compact matrix form. Firstly the affine transformation matrix  $T$

for a coordinate frame between the AUJ pivot and the centre of mass of the follower segment can be defined. The order of  $R_x$  and  $R_y$  can be reversed, but this requires other terms to be reversed as well.

$$T(\theta) = R_x(\theta_1) R_y(\theta_2) P_z(l_2) \quad (6)$$

Then the linear velocity jacobian  $J_v$  is simply the jacobian of the translation vector of  $T$ .

$$J_v(\theta) = \begin{bmatrix} \frac{\partial t_{14}}{\partial \theta_1} & \frac{\partial t_{24}}{\partial \theta_1} & \frac{\partial t_{34}}{\partial \theta_1} \\ \frac{\partial t_{14}}{\partial \theta_2} & \frac{\partial t_{24}}{\partial \theta_2} & \frac{\partial t_{34}}{\partial \theta_2} \end{bmatrix} \quad (7)$$

The angular velocity jacobian  $J_\omega$  is calculated using the first joint angle relative to the base frame, and the second in the frame of the first. If  $R_x$  is the first rotation in  $T$  then the first column of the jacobian is  $[100]^T$  (to represent the pitch angle) and the second column is  $R_x[010]^T$ .

$$J_\omega(\theta) = \begin{bmatrix} 1 & r_{x11} \\ 0 & r_{x21} \\ 0 & r_{x31} \end{bmatrix} \quad (8)$$

Then the mass matrix  $D$  can be created from the jacobians, the mass for the follower segment  $m$  and its inertia tensor  $I \in \mathbb{R}^{3 \times 3}$ , and  $R_x$  and  $R_y$  to express the inertia in the correct frame.

$$D(\theta) = m J_v^T J_v + J_\omega^T (R_x R_y) I (R_x R_y)^T J_\omega \quad (9)$$

The centrifugal/coriolis matrix  $C$  is created from the christoffel symbols of  $D$ , along with the AUJ velocity vector  $\dot{\theta}$ .

$$C(\theta, \dot{\theta})_{k,j} = \sum_{i=1}^N \frac{1}{2} \frac{\partial d_{kj}}{\partial \theta_i} + \frac{\partial d_{ki}}{\partial \theta_j} - \frac{\partial d_{ij}}{\partial \theta_k} \dot{\theta}_i \quad (10)$$

Then the gravity term  $G$ . As the gravity vector direction is the same as the  $z$  axis as in figure 1, the height is equal to  $-l_2 \cos \theta_1 \cos \theta_2$ , therefore the potential energy is  $mg(-l_2 \cos \theta_1 \cos \theta_2)$ . The jacobian of this then becomes the gravity term.

$$G(\theta) = \begin{bmatrix} \frac{\partial mg - l_2 \cos \theta_1 \cos \theta_2}{\partial \theta_1} \\ \frac{\partial mg - l_2 \cos \theta_1 \cos \theta_2}{\partial \theta_2} \end{bmatrix} \quad (11)$$

$D$ ,  $C$  and  $G$  are then combined to form the dynamics equation  $C_2$ , along with the AUJ position and velocity vectors.

$C_1$  is used as the acceleration term. This results in a setpoint joint torque which can be used in the optimisation algorithm.

$$C_2(C_1, \theta, \dot{\theta}) = D(\theta)C_1 + C(\theta, \dot{\theta})\dot{\theta} + G(\theta) \quad (12)$$

### C. TSA Force Optimisation Algorithm

This function uses a modified algorithm from [6] to select an optimal force vector from the desired joint torque. A force matrix  $F$  is created from the torque input  $C_2$ , jacobian  $J_\Lambda$  from the vector function  $\Lambda$  as defined in equation 1, and minimum force constant  $f_{min}$ .  $f_{ii}$  is equal to  $f_{min}$ , while the other elements in the column are based on a calculation using  $J_{\Lambda-i,*}$  where  $-i$  is a row removed from the matrix.

$$J_\Lambda = \begin{bmatrix} \frac{\partial \lambda_1}{\partial \theta_1} & \frac{\partial \lambda_2}{\partial \theta_1} & \frac{\partial \lambda_3}{\partial \theta_1} \\ \frac{\partial \lambda_1}{\partial \theta_2} & \frac{\partial \lambda_2}{\partial \theta_2} & \frac{\partial \lambda_3}{\partial \theta_2} \end{bmatrix}$$

$$F(C_2, \theta) = \begin{cases} f_{i,i} = f_{min} \\ f_{-i,i} = -J_{\Lambda-i,*}^\top (J_{\Lambda-i,*}^\top f_{min} + C_2) \end{cases} \quad (13)$$

$$= \begin{bmatrix} f_{min} & f_{12} & f_{13} \\ f_{21} & f_{min} & f_{23} \\ f_{31} & f_{32} & f_{min} \end{bmatrix}$$

Finally, the following algorithm selects one column of  $F$  to be the output force vector.

```

1:  $s \leftarrow [\top \ \top \ \top]$ 
2: if  $f_{23} > f_{min}$  then  $s_2 \leftarrow \perp$  else  $s_3 \leftarrow \perp$  end if
3: if  $f_{31} > f_{min}$  then  $s_3 \leftarrow \perp$  else  $s_1 \leftarrow \perp$  end if
4: if  $f_{12} \geq f_{min}$  then  $s_1 \leftarrow \perp$  else  $s_2 \leftarrow \perp$  end if
5: for  $i = 1$  to  $3$  do
6:   if  $s_i \rightarrow \top$  then  $C_3 \leftarrow f_{*,i}$  end if
7: end for

```

### D. TSA Force P Controller

This function is a P controller using the measured load cell forces  $f$ . The output from this can then be used to control the motor using three different control strategies implemented within the MDCD 3002 motor controller.

$$C_4(C_3, f) = K_{P_s}(C_3 - f) \quad (14)$$

1) *Direct Current Control (DCC)*: This mode takes a preset velocity  $\dot{\theta}_{set} \in [0, 4220]$  and uses a hardware PI controller with velocity feedback  $\dot{\theta}_{act}$  to generate a control voltage. This voltage  $V$  is then multiplied by the signum of the result from the cascade function in order to ensure the motor spins in the right direction, and then passed to a current limiter with the current error (the result with the actual current  $I_{act}$  subtracted) as the limit, before being sent to the motor. This ensures the motor stops spinning when the target current is reached.

$$\epsilon_c = \dot{\theta}_{set} - \dot{\theta}_{act}$$

$$V = \left( K_{P_c} \epsilon_c + K_{D_c} \int_0^t \epsilon_c \right) \text{sgn}(C_4(\dots)) \omega(C_4(\dots) - I_{act}) \quad (15)$$

TABLE I: Simulation and performance estimation coefficients.

Coefficient	Value	Coefficient	Value
$l_1$	45 mm	$J$	$1 \times 10^{-6} \text{ kg m}^{-2}$
$l_2$	600 $\mu\text{m}$	$K_L$	1000 $\text{N m}^{-1}$
$r$	13 mm	$f_{min}$	1 N
$l_n$	60 mm	$K_P$	800
$r_s$	200 $\mu\text{m}$	$K_I$	5000
$m$	72.619 13 g	$K_D$	50
$C$	0.1315 N mm	$K_{P_s}$	19
$K_t$	0.0263 $\text{N m A}^{-1}$	$\omega_s$	441.9 $\text{rad s}^{-1}$
$\alpha_s$	$1 \times 10^5 \text{ rad s}^{-2}$	$I_s$	0.19 A
$\tau_s$	4.5 mN m		

Where  $\omega(\dots) \in [0, 1]$  is an unknown hardware limiting function that controls the motor speed depending on the current error.

2) *P Current Controller*: This strategy is a more direct method of current control, using a software P controller to directly set the voltage of the motor, using the MDCD 3002 as simply a passive amplifier. In this case the current error is passed directly to a P controller which has its output limited to prevent damage to the motors.

$$V = K_{P_c} C_4(\dots) - I_{act} \quad (16)$$

3) *Velocity Control*: This strategy simply uses the result from the cascade function as a velocity setpoint using the hardware velocity PI controller as in the **Direct Current Control! (Direct Current Control!)**.

$$V = K_{P_c} \epsilon_c + K_{D_c} \int_0^t \epsilon_c \quad (17)$$

## III. SIMULATION RESULTS

To design and refine the parameters of the control system, a Simscape Multibody™ model of the antagonistic triad and control system was created in MATLAB®/Simulink™. This allowed for model design coefficients  $l_{1,2}$  and controller gains  $K_P, K_I, K_{P_s}$  to be modified in order to have the most stable control within design limits. Plots of a test joint trajectory can be seen in figure 4 with the parameters from table I.

### A. TSA State Space Definition

In order to approximate a TSA plant from within a simulation, a state space model was required which takes motor current  $u$  as an input and outputs  $y$  as the TSA tension force  $f_i$ . [4] defines it as such, where  $J$  is the motor inertia,  $C$  is the motor coulomb friction (modified from viscous friction as the 1724TSR only has dry friction),  $K_t$  is the motor torque constant, and  $K_L$  is the load stiffness. As the original definition is for a fixed load  $l_u$  distance from the motor a modified model is required which takes into account the varying length between the motor and load defined by  $\Lambda(\theta)$ . A saturation function is used to prevent incorrect compression forces when the string is slack. All of the motor coefficients were taken from the Faulhaber 1724TSR datasheet [7] as this is the motor to be used in the experimental model. An

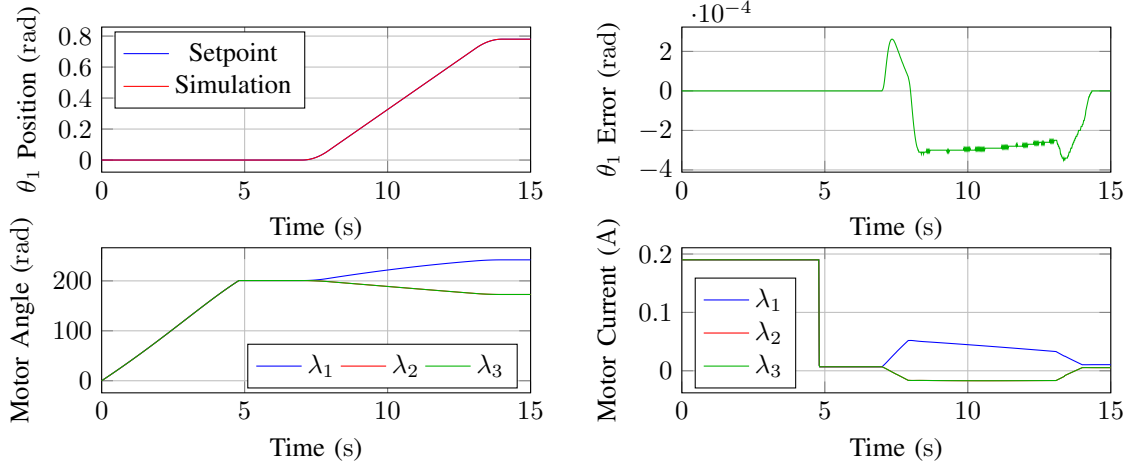


Fig. 4: Simulation results for a trajectory of  $\theta_1$  from 0 to  $\frac{\pi}{4}$ .

estimated value is used for the load stiffness, this was chosen to be a high number as the model is expected to be very stiff.

$$\begin{aligned}
 h(\theta_s) &= \frac{\theta_{r_s}^2}{\sqrt{l_u^2 - \theta_s^2 r_s^2}} \\
 k(\theta_s, \theta) &= \lambda_n(\theta) - \sqrt{l_u^2 - \theta_s^2 r_s^2} \\
 \dot{\mathbf{x}} &= \begin{bmatrix} x_2 \\ -\frac{K_L}{J} h(x_1) k(x_1, \theta) - \frac{B}{J} \text{sgn}(x_2) \end{bmatrix} + \begin{bmatrix} 0 \\ \frac{K_t}{J} \end{bmatrix} u \\
 y &= K_L \text{sat}_0^\infty k(x_1, \theta)
 \end{aligned} \tag{18}$$

The state space model was then adapted to include constraints on motor velocity and acceleration set by the motor controller in order to keep the motor within design limits, by replacing  $\dot{\mathbf{x}}$  with  $\dot{\mathbf{x}}'$  which contains saturation functions for maximum motor velocity  $v_s$  and acceleration  $\alpha_s$ .

$$\dot{\mathbf{x}}' = \begin{bmatrix} \text{sat}_{\omega_s} \dot{x}_1 \\ \text{sat}_{\alpha_s} \dot{x}_2 \end{bmatrix} \tag{19}$$

#### IV. EXPERIMENTAL RESULTS

For the experimental validation, a physical prototype of the mechanism was constructed with coefficients from table I as design parameters. The motors to be used would be Faulhaber 1724T024SR micromotors, selected for their compact size but high torque. These would be controlled by Fauhaber MCDC3002 motor controllers, which could interface with a National Instruments MyRIO via the USB port, using a USB to serial converter. The load cells would be Futek LCM100 miniature load cells, selected for their small size. The signals from these would be amplified using Flyde FE-359-TA instrumentation amplifiers and decoded using an external AD7606 ADC before being fed into the MyRIO using SPI.

##### A. TSA Control System & Motor Characterisation

Before verifying robust control of the AUJ, the control of each individual TSA needed to be tested in order to characterise the performance of the motors and to ensure the inner loop control system was robust. This would involve

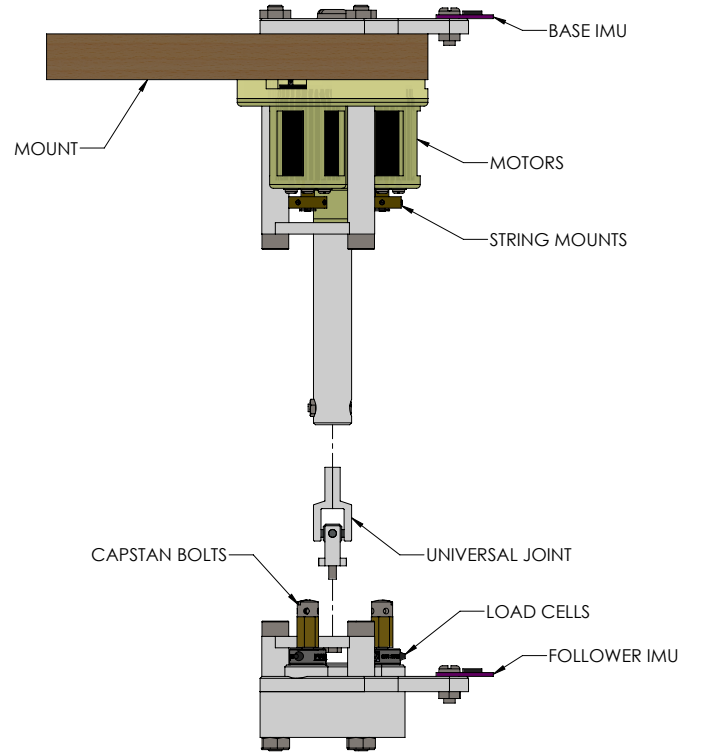


Fig. 5: Schematic of the experimental model.

selecting the control strategy that gave the best performance. A test trajectory consisting of a smooth ramp followed by a sine wave was fed into the inner loop of the cascade function as  $[f(t) \ f(t) \ f(t)]$ . Each control strategy was tested, and in the end the velocity control strategy proved most optimal, as is shown in figure 7.

#### V. CONCLUSION

##### REFERENCES

- [1] R. O. Buckingham and A. C. Graham, "Dexterous manipulators for nuclear inspection and maintenance — case study," in *2010 1st International Conference on Applied Robotics for the Power Industry*, 2010, pp. 1–6.

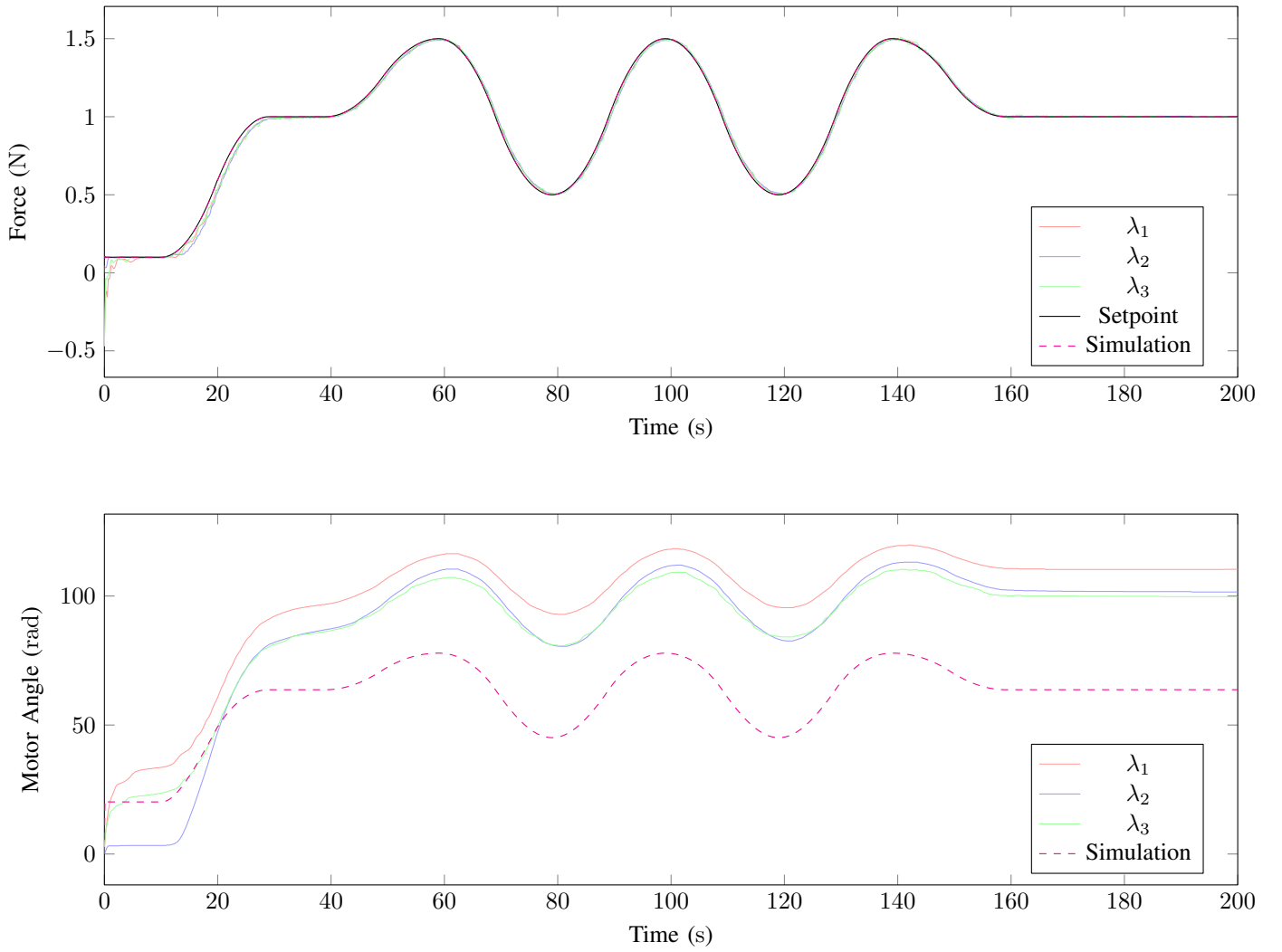


Fig. 6: Load cell plot from each string using the velocity control strategy.

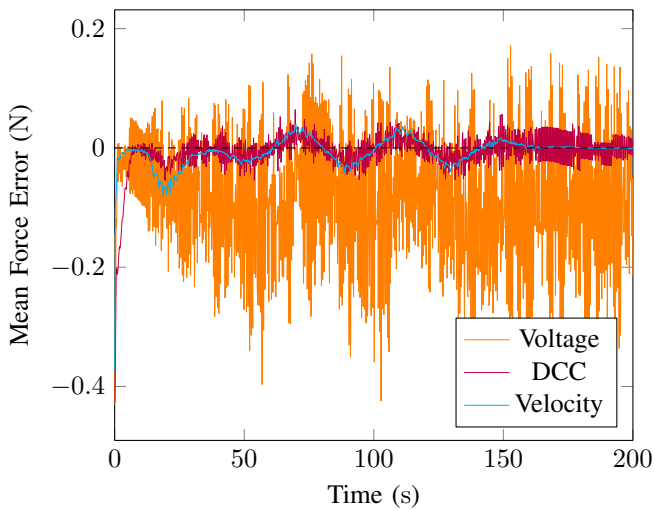
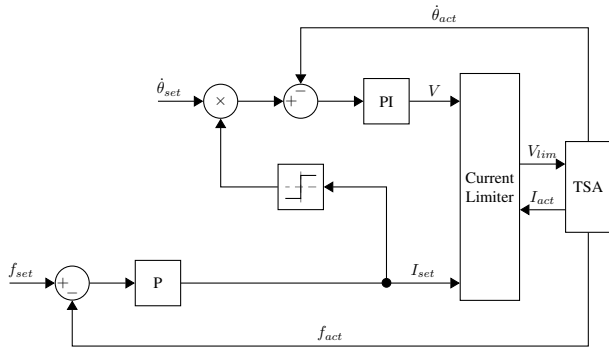
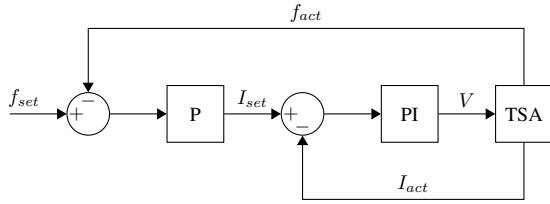


Fig. 7: Mean tracking error for each control strategy.

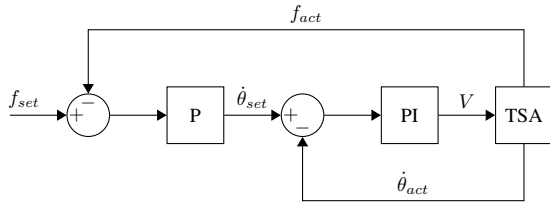
- [2] M. Luo, R. Yan, Z. Wan, Y. Qin, J. Santoso, E. H. Skorina, and C. D. Onal, "Orisnake: Design, fabrication, and experimental analysis of a 3-d origami snake robot," *IEEE Robotics and Automation Letters*, vol. 3, no. 3, pp. 1993–1999, 2018.
- [3] W. S. Rone, W. Saab, and P. Ben-Tzvi, "Design, Modeling, and Integration of a Flexible Universal Spatial Robotic Tail," *Journal of Mechanisms and Robotics*, vol. 10, no. 4, 04 2018, 041001. [Online]. Available: <https://doi.org/10.1115/1.4039500>
- [4] T. Würtz, C. May, B. Holz, C. Natale, G. Palli, and C. Melchiorri, "The twisted string actuation system: Modeling and control," in *2010 IEEE/ASME International Conference on Advanced Intelligent Mechatronics*, July 2010, pp. 1215–1220.
- [5] S. Nedelchev, I. Gaponov, and J. Ryu, "Accurate dynamic modeling of twisted string actuators accounting for string compliance and friction," *IEEE Robotics and Automation Letters*, vol. 5, no. 2, pp. 3438–3443, 2020.
- [6] F. Dessen, "Coordinating control of a two degrees of freedom universal joint structure driven by three servos," in *Proceedings. 1986 IEEE International Conference on Robotics and Automation*, vol. 3, April 1986, pp. 817–822.
- [7] *DC Micromotors - Precious Metal Commutation*, Dr. Fritz Faulhaber GmbH & Co. KG, 2 2020. [Online]. Available: [https://www.faulhaber.com/fileadmin/Import/Media/EN\\_1724\\_SR\\_DFF.pdf](https://www.faulhaber.com/fileadmin/Import/Media/EN_1724_SR_DFF.pdf)



(a) Direct Current Control



(b) P Current Controller



(c) Velocity Controller

Fig. 8: Block diagrams of each control strategy.



**Damian J. Crosby** is a PhD student in the school of Mechanical, Aerospace and Civil Engineering, University of Manchester, Manchester, U.K. He received a B.Sc. in Special Effects Development from The University of Bolton, U.K., in 2010, and a M.Res. in Robotics from The University of Plymouth, U.K., in 2012. He worked as a Research Technician at The University of Manchester from 2013 to 2017, before commencing his PhD.



**Dr. Andrew Weightman** graduated in 2006 with a PhD in Mechanical Engineering from the University of Leeds. Whilst at the University of Leeds he developed rehabilitation robotic technology for improving upper limb function in adults and children with neurological impairment which was successfully utilised in homes, schools and clinical settings. In 2013 he moved to the University of Manchester, School of Mechanical, Aerospace and Civil Engineering as a Lecturer in Medical Mechatronics. Dr Weightman has research interests in biomimetic mobile robotics, rehabilitation robotics, robotics for nuclear decommissioning and collaborative robotics.



**Joaquin Carrasco** is a Lecturer at the School of Electrical and Electronic Engineering, University of Manchester, UK. He was born in Abarn, Spain, in 1978. He received the B.Sc. degree in physics and the Ph.D. degree in control engineering from the University of Murcia, Murcia, Spain, in 2004 and 2009, respectively. From 2009 to 2010, he was with the Institute of Measurement and Automatic Control, Leibniz Universitt Hannover, Hannover, Germany. From 2010 to 2011, he was a research associate at the Control Systems Centre, School of Electrical and

Electronic Engineering, University of Manchester, UK.



**William P. Heath** is Chair of Feedback and Control in the School of Electrical and Electronic Engineering, University of Manchester, Manchester, U.K. He received the B.A. and M.A. degrees in mathematics from Cambridge University, U.K., in 1987 and 1991, and the M.Sc. and Ph.D. degrees in systems and control from the University of Manchester Institute of Science and Technology, U.K., in 1989 and 1992, respectively. He was with Lucas Automotive from 1995 to 1998 and was a Research Academic at the University of Newcastle, Australia from 1998 to 2004. His research interests include absolute stability, multiplier theory, constrained control, and system identification.